Int. J. Nonlinear Anal. Appl. In Press, 1–17
ISSN: 2008-6822 (electronic)
http://dx.doi.org/10.22075/ijnaa.2024.36112.5348

Scattering effect of twin tunnels on adjacent monuments subjected to far-field earthquakes

Meysam Azadmanesh[a], Hamidreza Vosoughifar[a,*], Masoud Amelsakhi[b], Arash Razmkhah[a], Hamid Alielahi[c]

[a]*Department of Civil Engineering, South Tehran Branch, Islamic Azad University, Tehran, Iran*

[b]*Department of Civil Engineering, Qom University of Technology, Qom, Iran*

[c]*Department of Civil Engineering, Zanjan Branch, Islamic Azad University, Zanjan, Iran*

(Communicated by Asadollah Aghajani)

Abstract

The majority of previous research stated that the seismic response of structures adjacent to tunnels during an earthquake might differ from that of structures further away from tunnels. However, this issue is not addressed in the relevant codes for process design. This study used Hankel functions to evaluate the seismic response of structures adjacent to tunnels subjected to far-field earthquakes. The authors of this paper used MATLAB to create a new model called FESCAM. Bessel function transform theories and numerical analyses were applied to design numerical solutions in the proposed model. An integrated approach can accomplish the analysis of plane pressure waves (P-waves) in twin circular tunnels regarding scattering waves. The case study was selected as the Karim Khan Citadel and the adjacent subway tunnels. The numerical simulation was conducted in two distinct scenarios: with and without twin tunnels. The results indicate that the maximum scattering occurred when the incoming wave angle was $\alpha = 30^\circ$, and the tunnel angle was $\theta = 90^\circ$. The overall results suggest no statistically significant difference between the two case study scenarios. When considering the citadel with and without twin tunnels, the horizontal and total displacements varied between 2.2-33.7% and 2.1-23.7 percent, respectively.

Keywords: Scattering waves, twin tunnels, monuments, far-field earthquake
2020 MSC: 00A06

1 Introduction

Due to rapid population growth and increasing transportation challenges, underground structures have become essential infrastructure in developing countries [22]. In many densely populated cities, underground tunnels are often designed and constructed as separate twin tunnels arranged horizontally to alleviate traffic congestion. The construction of tunnels in urban areas has become an undeniable necessity to address the growing demand for traffic management [35]. These tunnels facilitate smooth and uninterrupted traffic flow in areas where surface construction is not feasible due to high population density or space limitations [29]. Underground spaces also provide the opportunity to relocate certain surface functions underground, thereby freeing up surface areas for other urban needs and enhancing

*Corresponding author
Email addresses: azadmanesh.meysam@gmail.com (Meysam Azadmanesh), vosoughifar@gmail.com (Hamidreza Vosoughifar), mamelsakhi@yahoo.com (Masoud Amelsakhi), a_Razmkhah@AZAD.AC.IR (Arash Razmkhah), h.alielahi@gmail.com (Hamid Alielahi)

Received: December 2024 *Accepted:* February 2025

the quality of urban life [14]. Moreover, the diverse applications of underground structures, especially in transportation systems such as metro lines, railways, highways, as well as in water supply and wastewater management, further emphasize their significance [25].

Technological advancements in tunnelling and underground construction have not only simplified the construction process but have also enabled the extensive utilization of these structures in more complex conditions. These advancements have drawn significant attention from many countries, including Iran, to the development of tunnels for various applications such as civil, military, mining, and other strategic purposes [26]. In addition to single tunnels, multi-tunnel systems, including twin tunnels and triple sets, have garnered greater attention due to their high flexibility and enhanced capacity for managing traffic loads. However, the design and construction of these tunnels in seismically active regions require meticulous studies and special considerations. In such areas, seismic forces can significantly impact the behaviour of underground structures and adjacent surface buildings, potentially leading to their failure. Therefore, conducting precise seismic analyses and employing modern seismic-resistance technologies in tunnel design are essential to ensure their safety and efficiency [25].

These structures are highly susceptible to excessive settlement, displacement, and severe damage during seismic events. Seismic waves, such as primary (P) and secondary (S) waves, can rapidly affect underground structures, leading to differential displacements in adjacent structures [5]. Evaluating the impact of underground structures, such as tunnels, on nearby structures during both excavation and earthquakes is of critical importance. Given the increasing use of underground spaces and structures, these constructions are now regarded as vital lifelines in modern societies [26]. Meanwhile, the placement of some tunnels in regions with high seismic potential increases their vulnerability to damage and failure. Such failures, caused by earthquake-induced vibrations, can also lead to the collapse of adjacent surface structures. Therefore, in addition to withstanding static loads, these structures must possess adequate resistance to dynamic loads resulting from seismic activity. Historical evidence and the observed effects of earthquakes on underground structures indicate that the extent of damage to such structures is significantly less compared to surface-level structures [7].

Based on experiences from past earthquakes, it has been established that deep underground structures, such as metros and tunnels, as well as the surface structures located above them, have a high potential for destruction and disruption during seismic events [30]. This issue becomes even more critical when the immense material and immaterial values of historical structures are considered. Currently, nearly 40 cultural heritage sites in seismically active regions of Iran have suffered significant damage [32]. When irregular areas, such as cavities or underground structures, disrupt part of the seismic wave path while other parts of the wave continue to propagate through the medium, this phenomenon is referred to as "scattering." This scattering occurs due to differences in the properties of the primary medium and the irregular underground features present [21]. The scattering of seismic waves can significantly influence the intensity and amplitude of ground vibrations. Under these conditions, surface and underground structures may be affected unevenly. This is especially important in urban areas where structural and infrastructure density is high [31].

Regarding historical structures, their vulnerability is significantly higher due to their age, the materials used, and traditional construction methods. Studies indicate that earthquake-induced forces, through phenomena such as local amplification and resonance, can have a detrimental impact on cultural heritage [37]. The preservation of historical structures and cultural heritage is of paramount importance due to their unique material, spiritual, and identity values. These structures are often more susceptible to seismic forces because of their age, traditional materials, and non-engineered construction methods [32].

The phenomenon of seismic wave scattering in complex environments, including the presence of twin tunnels, can lead to local changes in the amplitude and frequency of vibrations. These effects may create additional forces or stress concentrations in adjacent historical structures, increasing the risk of their damage. The significance of this issue is further amplified when far-field earthquakes, with their long-period waves and scattering characteristics, have more extensive effects on large areas and sensitive structures [8]. Research on the interaction between twin tunnels and historical structures under the influence of far-field earthquakes can lead to a better understanding of vulnerability mechanisms and provide effective design and retrofitting solutions. The use of advanced modelling and numerical analyses in these studies offers valuable tools for predicting the behaviour of complex soil-structure systems [31]. On the other hand, recent earthquakes, such as the 1995 Kobe earthquake in Japan, the 1995 Chi-Chi earthquake in Taiwan, and the 1999 İzmit earthquake in Turkey, clearly demonstrated that such structures can also suffer significant damage when exposed to seismic waves. [3] In this context, the source location effect emerges as one of the most important and influential parameters during an earthquake. Its significance has led to a growing interest among researchers to conduct more detailed investigations in this area. Therefore, understanding the precise surface behaviour in the presence of underground tunnels, using appropriate tools, is considered a fundamental study that must be considered before construction, especially in high-priority urban areas [6].

As a foundational study, Pao et al. [27] investigated wave diffraction around a cylindrical cavity in an infinite medium, where the wave function expansion and the associated stress distribution were computed. Lee et al. [18] examined the response of twin tunnels subjected to horizontally polarized shear (SH) wave propagation in a semi-infinite medium, utilizing the coordinate transformation method. Antonio et al. [4] analyzed three-dimensional wave scattering involving cylindrical compound cavities in an elastic formation under a wide frequency range. Wang et al. [34] evaluated the dynamic stress concentration around elliptical cavities in saturated poroelastic soil under harmonic plane wave excitation. Esmaeili et al. [9] explored the dynamic response of circularly lined tunnels subjected to plane harmonic waves.

Moore and Guan [24] analyzed the response of P and SV waves in twin circular cavities within a specific configuration. Karakostas and Manolis [15] employed the boundary element method (BEM) to investigate the dynamic response of underground cavities subjected to shear wave propagation, with a focus on stress distribution around the cavities. Dravinski and Yu [8] utilized the direct boundary integral equation method to study the scattering of harmonic SH waves by a set of cavities with varying shapes and depths in a half-space. Their findings revealed that ground surface displacement in the presence of cavities is significantly influenced by wave frequency and cavity geometry. Vosoughifar et al. [33] examined the scattering of seismic waves beneath the Si-o-Se Pol Bridge in Esfahan, which overlies a subway tunnel, using the Hankel function. They calculated the dynamic stress concentration factor (DSCF) for comparative analysis via the finite element method (FEM). Tsaur and Chang [32] conducted an analytical investigation into wave scattering in the presence of buried cavities. They analyzed the scattering of plane SH waves incident on a tunnel cross-section using the imaging method. Furthermore, they calculated key parameters, including the dimensionless depth-to-ground cavity ratio, variations in dimensionless frequency, and the angle of wave incidence relative to the horizontal axis. Their study highlighted the effects of these parameters on free-surface ground motion. Additionally, they explored the frequency-domain response of the ground and cavity, providing detailed insights into surface and subsurface displacement distributions.

Parvanova et al. [28] investigated SH wave scattering by buried tunnels with linings in an elastic half-space. Their research provided advanced numerical results for both single and twin tunnels, including synthetic seismograms and three-dimensional frequency-domain responses. They also analyzed the effects of parameters such as wave incidence angle, frequency range, tunnel depth, and twin tunnel spacing on seismic responses. Alielahi et al. [3] examined the seismic behaviour of parallel twin tunnels under vertical plane waves using the boundary element method in the time domain. Assuming linear elastic material properties and the presence of P and SV waves, they evaluated the influence of various parameters, including wavelength, burial depth, and tunnel spacing, on ground amplification patterns above the tunnels.

Khabbaz et al. [16] studied the effects of twin tunnels beneath historic and modern structures in Sydney's Central Business District (CBD). Using a finite element method (FEM) model, they predicted the interactions between tunnel structures and pile foundations, highlighting a strong correlation between tunnel depth and liner stresses. Earlier studies of horizontally aligned parallel twin tunnels with circular cross-sections under horizontal shear (SH) waves included Hasheminejad and Avazmohammadi [11], who explored the dynamic interaction of time-harmonic plane waves with a pair of parallel circular cylindrical cavities in a poroelastic medium. Their analytical and numerical results considered scenarios with both empty cavities and lined twin tunnels excited by compressional or shear waves.

Li et al. [19] proposed a theoretical method to predict underground tunnel behaviour, incorporating factors such as particle peak velocity and stress distribution. Recently, Fang et al. [10] used a semi-analytical approach to assess natural hazards arising from the interaction of imperfect surfaces in closely spaced twin tunnels subjected to P waves. Their work focused on stress concentration, displacement distribution, and seismic response in twin tunnel systems. Liu and Wang [20] presented an analytical solution for the scattering of plane harmonic P and SV waves by closely spaced circular twin tunnels in a fully elastic medium. Their numerical results indicated that the spacing between twin tunnels and the frequency of incident waves significantly influence tunnel dynamic responses. Existing studies underscore that the impact of earthquakes on underground structures, particularly twin tunnels located near the surface and historical structures, remains a critical and complex area of research. Past seismic events have shown that underground structures, especially twin tunnels, can suffer significant damage and structural disruptions during severe earthquakes [36]. With the growing incidence of damage caused by major earthquakes, investigating the seismic behaviour of tunnels and their influence on surface structures, particularly historically significant landmarks, has become increasingly important [1].

Numerous analytical and numerical studies have investigated the response of tunnels and underground cavities to seismic waves. While analytical methods have proven effective in understanding the preliminary behaviour of simple systems, they face notable limitations in modelling complex material properties and irregular geometries. As a result, numerical methods such as the Finite Element Method (FEM) and Integral Equation Methods are widely employed, especially for analyzing stresses and displacements around tunnels [13]. Existing research has highlighted that factors such as tunnel depth, spacing between tunnels, and the frequency of incident waves can significantly influence the stress distribution and dynamic response of underground structures [2, 23, 12].

Despite advancements in this field, significant gaps remain in comprehending the precise phenomena of seismic wave scattering caused by twin tunnels and their impact on adjacent historical structures. Few studies have thoroughly examined the complex interaction between seismic waves and twin tunnels and their effects on the stability of historical structures during far-field earthquakes. This study aims to address these research gaps by performing a two-dimensional dynamic analysis of the interaction between two unlined parallel tunnels, horizontally embedded in an elastic medium, under vertical P and SV waves. The main objectives of this research include investigating the effect of tunnel spacing and burial depth on the seismic response of the ground, analyzing the influence of wavelength and incident wave fields on stress distribution and displacement in the subsurface and adjacent structures, and providing preliminary guidelines and simplified tables for revising the design spectra of surface structures located above underground structures, such as metro tunnels and circular cavities. This research has the potential to propose effective strategies for the design and retrofitting of underground and historical structures against seismic effects, contributing to enhanced safety and structural resilience.

2 Theory

The geometry of the problem is illustrated in Figure 1, where two parallel circular tunnels are embedded within an elastic half-space. The arrangement represents twin tunnels located at a specified distance from each other and the ground surface. These twin tunnels are assumed to have a uniform circular cross-section, and their center-to-center spacing, depth, and diameter are parameters that influence the seismic wave scattering effect. This geometry simulates the conditions near historical structures where such tunnels are present, affecting seismic wave propagation and potentially amplifying ground motion near sensitive buildings.

$$\varphi_{f,s}^{(i)} = \sum_{n=-\infty}^{\infty} \gamma_n^{(i)} J_n\left(k_{f,s} r_i\right) e^{in\theta_i} \qquad (j=1,2) \tag{2.1}$$

$$\begin{aligned} \phi_f^{(i)} &= \sum_{n=-\infty}^{\infty} A_n^{(i)}(\omega) H_n(k_f r_i) e^{in\theta_i} \\ \phi_s^{(i)} &= \sum_{n=-\infty}^{\infty} B_n^{(i)}(\omega) H_n(k_s r_i) e^{in\theta_i} \end{aligned} \tag{2.2}$$

$$\psi^{(i)} = \sum_{n=-\infty}^{\infty} C_n^{(i)}(\omega) H_n(k_t r_i) e^{in\theta_i} \tag{2.3}$$

where H_n denotes the cylinder Bessel function of the first kind [10]. As a result, a scattered wave in a porous medium with hollow cavities is generally expressed as follows:

$$\begin{aligned} \phi &= \phi_f^{(i)} + \phi_s^{(i)} + \phi_f^{(j)} + \phi_s^{(j)} + \varphi_{f,s}^{(i)} \\ &= \sum_{n=-\infty}^{\infty} \begin{bmatrix} A_n^{(i)}(\omega) H_n\left(k_f r_i\right) + B_n^{(i)}(\omega) H_n\left(k_s r_i\right) \\ +\gamma_n^{(i)} J_n\left(k_{f,S} r_i\right) \end{bmatrix} e^{in\theta_i} + \sum_{n=-\infty}^{\infty} \left[A_n^{(j)}(\omega) H_n(k_f r_i) + B_n^{(j)}(\omega) H_n(k_s r_j)\right] e^{in\theta_j} \end{aligned} \tag{2.4}$$

$$\psi = \psi^{(i)} + \psi^{(j)} = \sum_{n=-\infty}^{\infty} C_n^{(i)}(\omega) H_n(k_t r_i) e^{in\theta_i} + \sum_{n=-\infty}^{\infty} C_n^{(j)}(\omega) H_n(k_t r_j) e^{in\theta_j} \tag{2.5}$$

2.1 Boundary conditions and wave transmission (summary)

When seismic waves hit a porous medium, boundary conditions based on Biot's equations are applied to ensure continuity of displacement, stress, and pressure across the boundary. This allows for accurate modelling of wave transmission and scattering, essential for analyzing how waves interact with structures like twin tunnels. The conditions include:

Displacement Continuity: Matching the solid and fluid displacements at the boundary.

Stress Continuity: Balancing stress across the boundary interface.

Pressure Equilibrium: Ensuring fluid pressure continuity.

These conditions affect wave behaviours such as transmission, reflection, mode conversion (e.g., P-wave to S-wave), and attenuation. Within twin tunnels, wave interference patterns can amplify or dampen ground motion, influenced by tunnel geometry and material properties. Numerical methods (e.g., FEM, BEM) solve these conditions iteratively to model seismic impacts on nearby structures accurately.

$$\sigma_{rr}^{(i)}\,|r_{i=a,b} \;= 0 \tag{2.6}$$

$$\sigma_{r\theta}^{(i)}\,|r_{i=a,b} \;= 0 \tag{2.7}$$

$$\dot{w}_r^{(i)}\,|r_{i=a,b} \;= k_s p_p^{(i)}\,|r_{i=a,b} \tag{2.8}$$

where $\dot{w}_r = \phi_0\left(\dot{U}_r - \dot{u}_r\right)$ denote the velocity parameter, while $0 \leq k_s \leq \infty$ represents penetration into the surface. To meet the perpendicularity condition, cavity function (r_j, θ_j) is written based on cavity parameters (r_i, θ_i) as [20]:

$$H_n\left(kr_i\right)e^{in\theta_i} = \sum_{m=-\infty}^{\infty} H_{n-m}(kd)J_m\left(kr_j\right)e^{i(n-m)\theta_{i,j}+im\theta_j} \tag{2.9}$$

where $\theta_{ij}(i,j=1,2,i\neq j)$ denote the angle between line O_jO_i and axis x_i. Therefore, $\theta_{12}=0$ and $\theta_{21}=\pi$. As a result, the total potential function is rewritten based on the coordinate system of tunnel i as:

$$\begin{aligned}\phi\left(r_i,\theta_i,\omega\right) = &\sum_{n=-\infty}^{\infty}\left[A_n^{(i)}(\omega)H_n\left(k_f r_i\right) + B_n^{(i)}(\omega)H_n\left(k_s r_i\right) + \gamma_n^{(i)}(\omega)J_n\left(k_{f,s} r_i\right)\right]e^{in\theta_i}\\ &+ \sum_{n=-\infty}^{\infty}\sum_{m=-\infty}^{\infty}\begin{bmatrix}A_n^{(i)}(\omega)H_{n-m}\left(kd\right)J_n\left(k_f r_i\right)\\ +B_m^{(i)}(\omega)H_{n-m}(kd)J_n\left(k_s r_i\right)\end{bmatrix}e^{i(n-m)\theta_{ij}+in\theta_i}.\end{aligned} \tag{2.10}$$

Then, the combination and simplification of the equations and boundary conditions are expressed as:

$$\begin{aligned}&T_{f,s}^1(k_{f,s}r_i) + A_n^{(i)}k_f^2\left[a_f H_n(k_f r_i) + 2\mu H''{}_n(k_f r_i)\right] + B_n^{(i)}k_s^2\left[a_s H_n(k_s r_i) + 2\mu H''{}_n(k_f r_i)\right]\\ &+ (2i\mu/r_i^2)C_n^{(i)}n\left[k_t r_i H'{}_n(k_t r_i) - H_n(k_t r_i)\right]\\ &+ \sum_{m=-\infty}^{\infty} A_m^{(i)}H_{n-m}\left(k_f d\right)k_f^2\left[a_f J_n\left(k_f r_i\right) + 2\mu J''{}_n\left(k_f r_i\right)\right]e^{i(n-m)\theta_{ij}}\\ &+ \sum_{m=-\infty}^{\infty} B_m^{(j)}H_{n-m}\left(k_s d\right)k_s^2\left[a_s J_n\left(k_s r_i\right) + 2\mu J''{}_n\left(k_s r_i\right)\right]e^{i(n-m)\theta_{ij}}\\ &+ \sum_{m=-\infty}^{\infty} C_m^{(i)}H_{n-m}\left(k_t d\right)\left(2i\mu/r_i^2\right)n\times\left[k_t r_i J'{}_n\left(k_t r_i\right) - J_n\left(k_t r_i\right)\right]e^{i(n-m)\theta_{ij}} = 0\end{aligned} \tag{2.11}$$

$$\begin{aligned}&T_{f,s}^2\left(k_{f,s}r_i\right) + 2iA_n^{(i)}n\left[k_f r_i H'{}_n\left(k_f r_i\right) - H_n\left(k_f r_i\right)\right] + 2iB_n^{(i)}n\left[k_s r_i H'{}_n\left(k_s r_i\right) - H_n\left(k_s r_i\right)\right]\\ &+ C_n^{(i)}\left[\left(-n^2\right)H_n\left(k_t r_i\right) + k_t r_i H'{}_n\left(k_t r_i\right) - k_t^2 r_i^2 H''{}_n\left(k_t r_i\right)\right]\\ &+ \sum_{m=-\infty}^{\infty} A_m^{(j)}H_{n-m}\left(k_f d\right)2in\times\left[k_f r_i J'{}_n\left(k_f r_i\right) - J_n\left(k_f r_i\right)\right]e^{i(n-m)\theta_{ij}}\\ &+ \sum_{m=-\infty}^{\infty} B_m^{(j)}H_{n-m}\left(k_s d\right)2in\times\left[k_s r_i J'{}_n\left(k_s r_i\right) - J_n\left(k_s r_i\right)\right]e^{i(n-m)\theta_{ij}}\\ &+ \sum_{m=-\infty}^{\infty} C_m^{(i)}H_{n-m}\left(k_t d\right)\left[\left(-n^2\right)J_n\left(k_t r_i\right) + k_t r_i J'{}_n\left(k_t r_i\right) - k_t^2 r_i^2 J''{}_n\left(k_t r_i\right)\right]e^{i(n-m)\theta_{ij}} = 0\end{aligned} \tag{2.12}$$

$$
\begin{aligned}
&T^3_{f,s}\left(k_{f,s}r_i\right) + A^{(i)}_n \left[i\omega\phi_0\left(1-\mu_f\right)k_f H'_n\left(k_f r_i\right) - K_s M b_f k_f^2 H_n\left(k_f r_i\right)\right] \\
&+ B^{(i)}_n \left[i\omega\phi_0\left(1-\mu_s\right)k_s H'_n\left(k_s r_i\right) - K_s M b_s k_s^2 H_n\left(k_s r_i\right)\right] \\
&- C^{(i)}_n \left[n\omega\phi_0\left(1-\alpha_0\right)/r_i\right] H_n\left(k_t r_i\right) \\
&+ \sum_{m=-\infty}^{\infty} A^{(j)}_m H_{n-m}\left(k_f d\right)\left[i\omega\phi_0\left(1-\mu_f\right)k_f J'_n\left(k_f r_i\right) - K_s M b_f k_f^2 J_n\left(k_f r_i\right)\right] e^{i(n-m)\theta_{ij}} \\
&+ \sum_{m=-\infty}^{\infty} B^{(j)}_m H_{n-m}\left(k_s d\right)\left[i\omega\phi_0\left(1-\mu_s\right)k_s J'_n\left(k_s r_i\right) - K_s M b_s k_s^2 J_n\left(k_s r_i\right)\right] e^{i(n-m)\theta_{ij}} \\
&- \sum_{m=-\infty}^{\infty} C^{(i)}_m H_{n-m}\left(k_t d\right)\left[n\omega\phi_0\left(1-\alpha_0\right)/r_i\right] \times J_n\left(k_t r_i\right) e^{i(n-m)\theta_{ij}} = 0
\end{aligned}
\tag{2.13}
$$

where $n = \cdots, -3, -2, -1, 0, 1, 2, 3, \cdots$, $i, j = 1, 2 (i \neq j)$, $r_1 = a$, $r_2 = b$, and $T^{1,2,3}_{f,s}\left(k_{f,s}r_i\right)$ is expressed for a slow/rapid incoming wave by:

$$
\begin{aligned}
&T^1_{f,s}\left(k_{f,s}r_i\right) = \gamma^{(i)}_n k^2_{f,s}\left[a_{f,s} J_n\left(k_{f,s}r_i\right) + 2\mu J''_n\left(k_{f,s}r_i\right)\right] \\
&T^2_{f,s}\left(k_{f,s}r_i\right) = \gamma^{(i)}_n 2in\left[k_{f,s}r_i J'_n\left(k_{f,s}r_i\right) - J_n\left(k_{f,s}r_i\right)\right] \\
&T^3_{f,s}\left(k_{f,s}r_i\right) = \gamma^{(i)}_n\left[i\omega\phi_0\left(1-\mu_{f,s}\right)k_{f,s} J'_n\left(k_{f,s}r_i\right) - K_s M b_{f,s} k^2_{f,s} J_n\left(k_{f,s}r_i\right)\right]
\end{aligned}
\tag{2.14}
$$

The dimensionless Dynamic Stress Concentration Factor (DSCF) was employed to represent scattering effects, as described in Equations (2.6-2.8). Parameters required for the numerical analysis were defined according to Biot's theory, as detailed in Table 1, with specific values for saturated sand provided in Table 2. In the nonlinear time-history analysis, earthquake input frequencies were applied within the FESCAM model. Unlike conventional methods that utilize harmonic waves, the FESCAM model calculates the DSCF at actual earthquake frequencies by using scaled frequency spectra derived from real earthquake data.

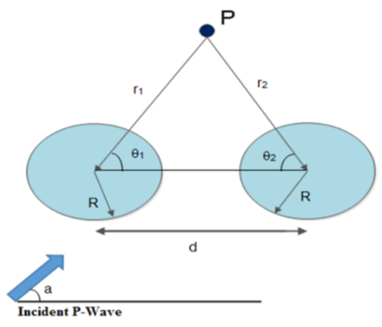

Figure 1: Twin tunnels and wave scattering parameter

3 Validation and case study

3.1 Case study

This study aimed to evaluate wave scattering in Shiraz, Iran's Karim Khan Citadel. The Karim Khan Citadel and the adjacent twin subway tunnels at Zand Underpass were selected as the case study. Karim Khan Citadel is depicted in Figure 2.

Karim Khan Citadel is a significant monument located in central Shiraz, Iran. Zand Underpass is a major underpass in Shiraz constructed 15 years ago. Shiraz Subway is Shiraz's rapid transit system. The building began construction in 2001 and was completed in October 2014. The Zand Underpass is depicted in Figure 3. The scattering effect is investigated in Shiraz's twin tunnels and adjacent structures. Figure 4 depicts a schematic of the tunnel and its surrounding structures.

Figure 2: Karim Khan Citadel

Figure 3: Zand Underpass

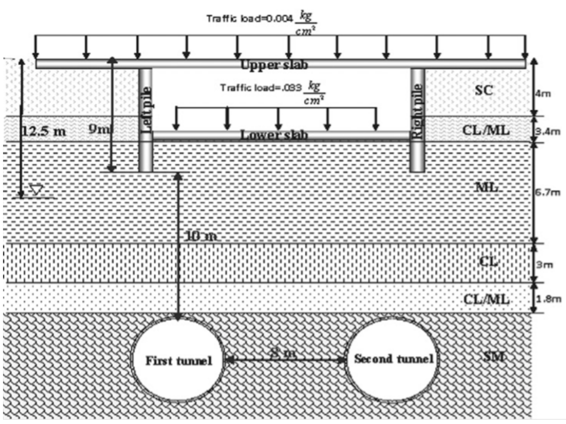

Figure 4: Relative positions of the twin tunnels and Zand Underpass, Karim Khan Citadel layers, and soil [36].

3.2 Validation

The FESCAM results are compared to Hasheminejad and Avazmohammadi [15] in Fig. 5.

3.3 SPSS results

FESCAM's output was compared to previous studies and validated using SPSS. The Mann-Whitney U test results for several examples are shown in Table 1.

Table 1: P-values of different examples

	Control Location above Earthquake-subjected Structure	Effects of the 1940 El Centro earthquake on the structure after tunnel	Effects of the 1940 El Centro earthquake on the structure before tunnel excavation
P-value	0.930	0.904	0.875

As can be seen, there was no statistically significant difference between the FESCAM results and those of Hasheminejad and Avazmohammadi [15].

3.4 Scattering results validation

To validate the scattering results, Figures 5 and 6 illustrate the scattering plots of Hasheminejad and Avazmohammadi [15] and FESCAM, respectively.

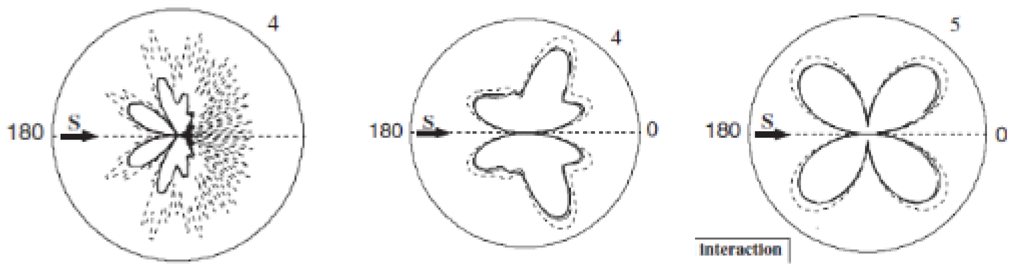

Figure 5: DSCF plots reported by Hasheminejad and Avazmohammadi [15].

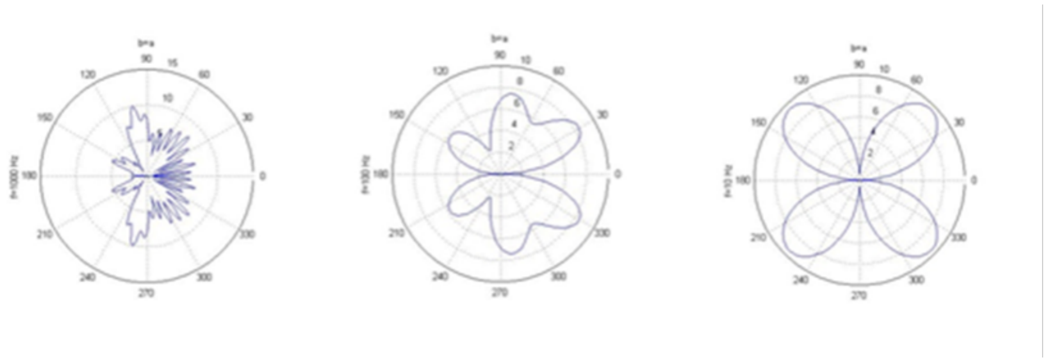

Figure 6: FESCAM scattering plots

4 Results

4.1 Stress and displacement results in the Karim Khan Citadel

The impact of tunnel-induced scattering on the Karim Khan Citadel was evaluated under far-field earthquake conditions. This study examines the displacement variations of the citadel in multiple directions due to far-field earthquakes by comparing pre- and post-tunnel displacements. The analysis integrates regional tectonics, site-specific hazard models, earthquake-inducing fault structures, subsurface layer characteristics, as well as the effects of soil granularity and alluvium. These factors contribute to simulating the dominant frequency and amplitude of earthquake responses. To maximize the dynamic response of the tunnel structure, accelerogram records were selected based on criteria such as peak ground acceleration (PGA), peak ground velocity (PGV), peak ground displacement (PGD), energy spectra, and effective duration. For this study, the Northridge, El Centro, and Chi-Chi earthquake records were employed as representative far-field events. The results for the horizontal and total displacement differences of the citadel, calculated between control points above and on the ground structure, are presented in Figures 7 and 8.

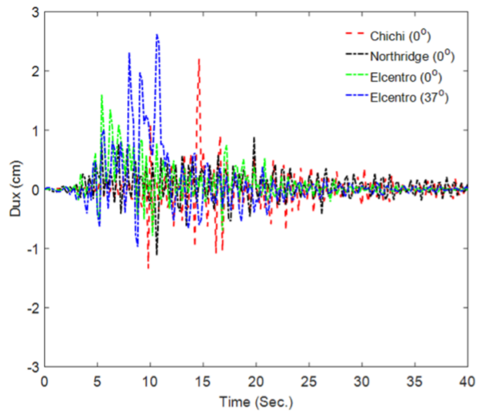

Figure 7: Horizontal displacement difference under far-field earthquakes in different directions

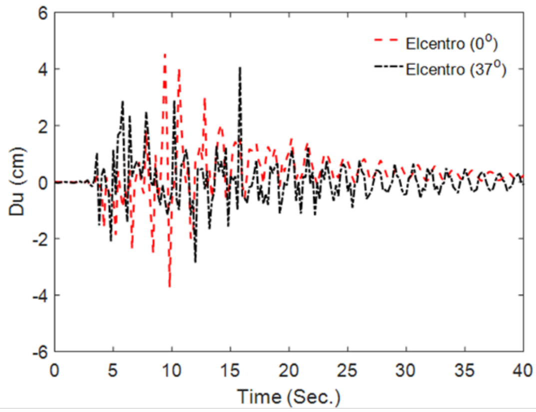

Figure 8: Total displacement difference under far-field earthquakes in different directions

Table 2: Parameters of Biot's theory in saturated sand

Parameter	Value
ϕ_0	0.37
α_∞	1.58
$\kappa(m^2)$	27.7×10^{-12}
$\rho_s(kg/m^3)$	2480
$K_s(N/m^2)$	4.99×10^{12}
$K_0(N/m^2)$	5.24×10^{11}
$\mu(N/m^2)$	3.26×10^{11}
$\rho_{fl}(kg/m^3)$	1000
$K_{fl}(N/m^2)$	2.25×10^{11}
$\eta(kg/ms)$	0.1
$\Lambda(m)$	19.4×10^{-6}

4.1.1 Stresses in the Karim Khan Citadel

The effects of tunnel excavation on citadel stresses in various directions under far-field earthquakes are plotted in Figures 9 and 10. Tables 4 and 5 report the stress difference.

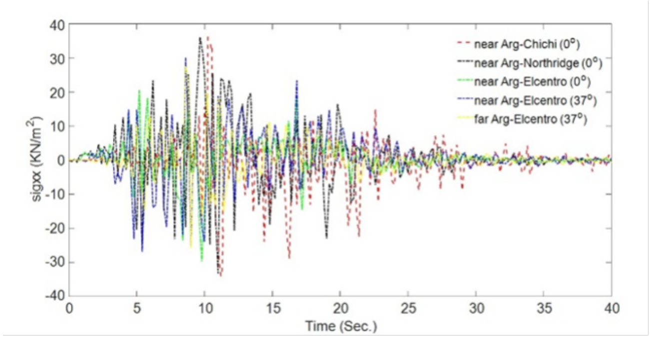

Figure 9: The sig-xx difference in the citadel (pre-and post-excavation) under far-field earthquakes in various directions.

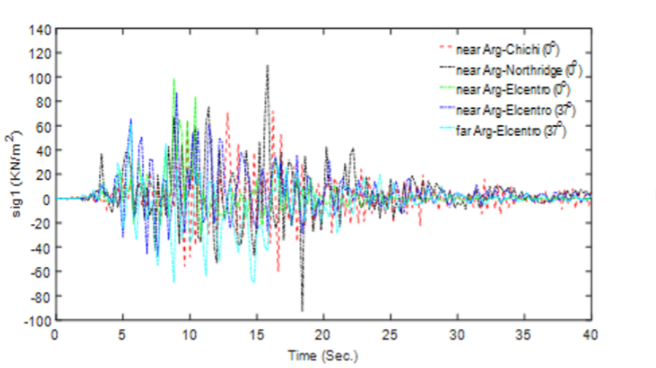

Figure 10: The sig-1 difference in the citadel (pre-and post-excavation) under far-field earthquakes in various directions.

4.2 Scattering effect under different earthquake frequencies

This section presents the FESCAM scattering of seismic waves and its effect under far-field earthquakes.

Table 3: Frequencies extracted from the records of the 1994 Northridge, 1940 El Centro, and 1999 Chi-Chi earthquakes (far-field)

Frequency	Fourier Amplitude (Northridge)	Fourier Amplitude (El Centro)	Fourier Amplitude (Chi-Chi)
0.1	0.003	0.000	0.000
1	0.017	0.005	0.010
10	0.002	0.003	0.004

Table 4: PGA frequencies of the 1994 Northridge, 1940 El Centro, and 1999 Chi-Chi earthquakes (far-field)

Earthquakes	$\text{Frequency}_{(\text{Peak Acceleration})}$	Fourier Amplitude
Northridge	1.221	0.819
El Centro	0.244	0.007
Chi-Chi	0.433	0.059

The analysis of Tables 3 and 4 reveals that the 1994 Northridge, 1940 El Centro, and 1999 Chi-Chi earthquakes exhibit distinct frequency characteristics and peak ground acceleration (PGA) frequencies, influencing their structural impact in far-field conditions. In Table 3, the Northridge earthquake shows the highest Fourier amplitude at 1 Hz, indicating concentrated energy at this frequency and suggesting a potentially stronger effect on structures. Conversely, lower (0.1 Hz) and higher frequencies (10 Hz) exhibit minimal Fourier amplitudes, indicating that primary energy was focused within mid-range frequencies.

In Table 4, Northridge also shows the highest PGA frequency (1.221 Hz) and Fourier amplitude (0.819), which poses a greater impact on structures sensitive to this frequency range. In contrast, the El Centro and Chi-Chi earthquakes have lower PGA frequencies (0.244 Hz and 0.433 Hz, respectively) and smaller Fourier amplitudes, indicating reduced seismic impacts on structures sensitive to higher frequencies. These findings highlight the importance of analyzing seismic frequency characteristics in designing structures that are resilient to different earthquake frequencies.

Table 5 lists the frequencies associated with the peak acceleration. Figures 11-16 illustrate scattering from various angles.

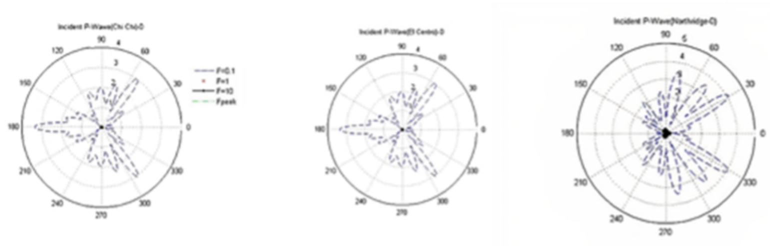

Figure 11: DSCF at $\alpha = 0°$ and different frequencies under the Northridge, El Centro, and Chi-Chi earthquakes

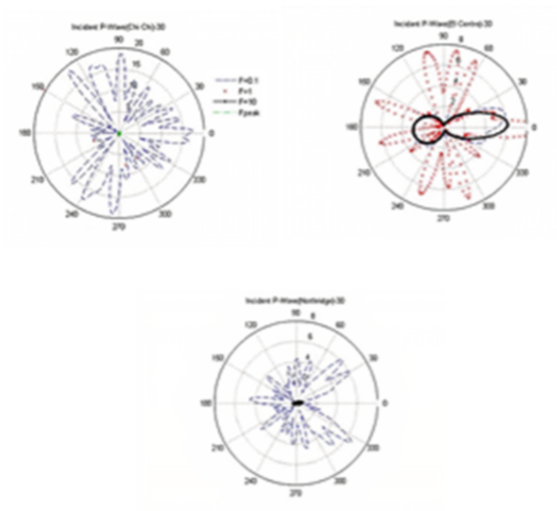

Figure 12: DSCF at $\alpha = 30°$ and different frequencies under the Northridge, El Centro, and Chi-Chi earthquakes

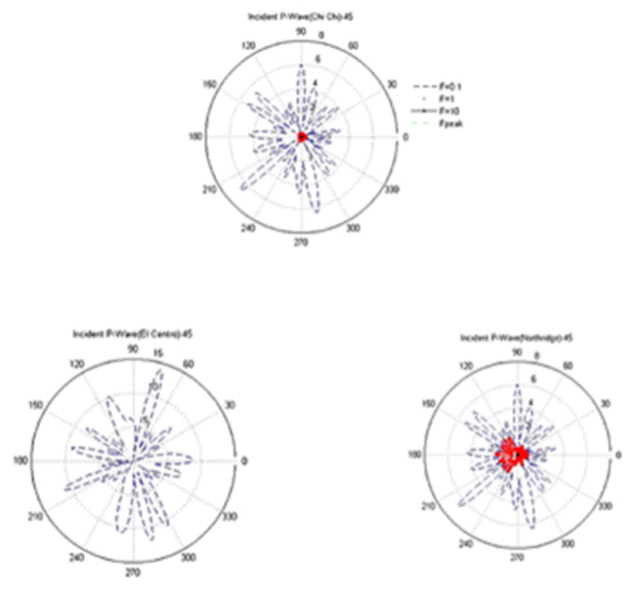

Figure 13: DSCF at $\alpha = 45°$ and different frequencies under the Northridge, El Centro, and Chi-Chi earthquakes

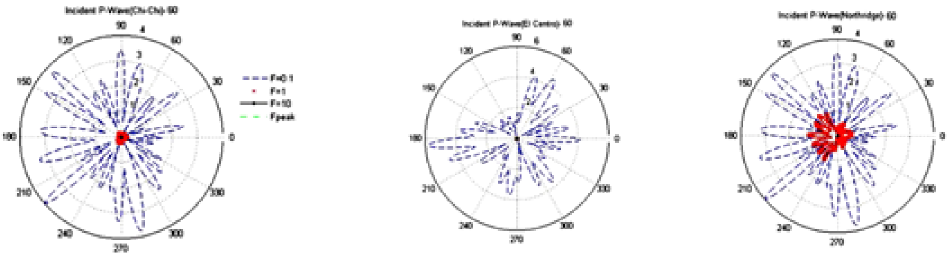

Figure 14: DSCF at $\alpha = 60°$ and different frequencies under the Northridge, El Centro, and Chi-Chi earthquakes

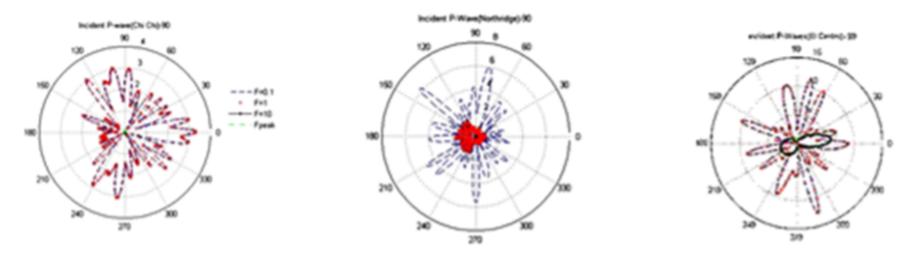

Figure 15: DSCF at $\alpha = 90°$ and different frequencies under the Northridge, El Centro, and Chi-Chi earthquakes

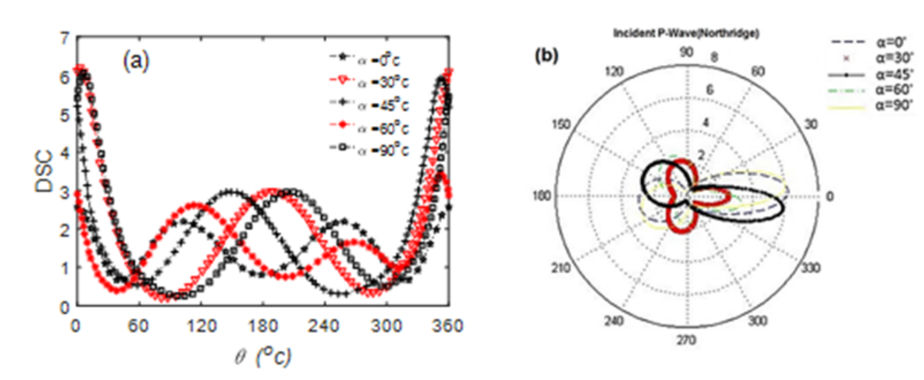

Figure 16: DSCF at different wave angles and the peak wave magnitude frequency under the Northridge earthquake

As illustrated in Figure 12, DSCF was calculated for various angles at the peak wave frequency, with the maximum scattering occurrence at $\alpha = 30°$ and $\theta = 90°$.

Table 5: Horizontal displacement differences under far-field earthquakes

	Chichi-0°	**Northridge-0°**	**El4 Centro-0°**	**El Centro-37°**
Post-excavation Horizontal Displacement	0.107	0.111	0.081	0.084
Pre-excavation Horizontal Displacement	0.080	0.099	0.079	0.074
Difference (%)	33.724	11.327	2.207	13.445

The analysis results indicate that excavation can significantly influence the increase in horizontal displacement of the structure under various earthquakes, with this effect depending on the earthquake type, wave characteristics, and incident angle. In the Chichi-0° earthquake, the greatest increase in horizontal displacement (33.72%) was observed, suggesting that the waves from this earthquake possess higher energy for inducing structural displacement post-excavation. This increase may be attributed to the specific characteristics of the Chichi earthquake waves, which make the structure more sensitive to displacement at this particular angle. In the Northridge-0° earthquake, the horizontal displacement increase was 11.33%, lower than that of the Chichi earthquake but still indicating a substantial effect of excavation on horizontal displacement. In addition to earthquake type, the incident angle of the waves is also a significant factor affecting the degree of horizontal displacement. For example, the El Centro-0° earthquake produced only a 2.21% increase in displacement, whereas the same earthquake at a 37-degree angle increased displacement to 13.45%. This discrepancy suggests that the incident angle of the waves can impact the structure's response to the earthquake, with certain angles potentially resonating more with the structural characteristics and leading to greater displacement [16]. Overall, excavation has led to an increase in horizontal displacement across all earthquakes studied, reflecting heightened sensitivity and vulnerability of the structure to seismic activity post-excavation. This increased displacement is likely due to changes in the underlying structure and soil profile caused by excavation, which result in greater structural movement in response to seismic waves. These findings underscore the necessity of considering excavation effects in seismic assessments, as doing so can support more optimal decision-making in the design and execution of civil engineering projects [11].

Table 6: Total displacement differences under far-field earthquakes.

	Chichi-0°	**Northridge-0°**	**El4 Centro-0°**	**El Centro-37°**
Post-excavation Total Displacement	0.072	0.102	0.080	0.068
Pre-excavation Total Displacement	0.062	0.099	0.078	0.055
Difference (%)	15.287	2.572	2.117	23.680

The analysis of Table 6 demonstrates that excavation has varying impacts on the total displacement of the structure under different far-field earthquakes, with the effect largely dependent on the type and incident angle of the earthquake. For the Chichi-0° earthquake, the total displacement increased from 0.062 to 0.072 post-excavation, representing a 15.287% change, indicating a significant rise in displacement due to excavation. This increase suggests that the structure is highly responsive to the waves from this earthquake post-excavation. In the Northridge-0° earthquake, the total displacement rose from 0.099 to 0.102, yielding only a 2.572% increase, which indicates that excavation had a relatively minor impact on the total displacement of the structure under this seismic event. For the El Centro-0° earthquake, total displacement increased marginally from 0.078 to 0.080, a 2.117% change, highlighting that excavation had minimal impact on the structure's displacement under this earthquake. In contrast, the El Centro-37° earthquake saw total displacement increase from 0.055 to 0.068 post-excavation, showing a 23.680% change the highest percentage increase among all earthquakes, indicating that the 37-degree angle of incidence significantly amplifies the structure's sensitivity to excavation [28].

Table 7: Sig-xx difference of the citadel foundation under far-field earthquakes.

	Chichi-0°	**Northridge-0°**	**El4 Centro-0°**	**El Centro-37°**
Post-excavation Sig-xx	-262.136	-308.92	-280.57	-411.39
Pre-excavation Sig-xx	-270.934	-301.1	-280.59	-400.76
Difference (%)	-3.25	2.60	-0.01	2.65

The analysis of Table 7 reveals differences in horizontal stress (Sig-xx) in the citadel foundation under far-field earthquakes before and after excavation. This information is crucial for evaluating stress variations and stability in large foundations, especially in seismically active regions. Horizontal stresses are key parameters in earthquake-resistant design, and recent research has shown the significant impact of excavation on these stresses and structural stability [1, 31, 33]. For the Chichi-0° earthquake, a 3.25% decrease in horizontal stress was noted after excavation, suggesting a redistribution of tensile forces that may enhance structural stability. Similar studies [15, 6]. have confirmed that under certain seismic conditions, reduced horizontal stress can help structures better resist earthquake forces. In contrast, the Northridge-0° earthquake shows a 2.60% increase in horizontal stress after excavation, indicating added horizontal pressure that could lead to foundation strain and potential structural deformation [13].

The El Centro-0° earthquake exhibited only a 0.01% change in horizontal stress, suggesting minimal excavation impact under these conditions. However, the El Centro-37° earthquake resulted in a 2.65% increase in horizontal stress, highlighting that wave incidence angles can significantly influence stress changes in excavated foundations [21, 8]. In summary, these findings indicate that excavation affects horizontal stresses in different ways depending on earthquake type and incidence angle. In some cases, excavation may reduce stresses and stabilize the structure, as seen in the Chichi-0° earthquake, while in others, such as Northridge-0° and El Centro-37°, increased stresses may reduce stability. The data emphasize the need to consider seismic activity and excavation effects together in design and planning to manage risks associated with increased horizontal stresses and potential stability challenges [11, 20, 32].

The analysis of the table depicting the primary stress (Sig-1) in the citadel foundation under different earthquake scenarios shows that excavation can have varying effects on foundation stability depending on the type and angle of

Table 8: Sig-1 difference of the citadel foundation under far-field earthquakes.

	Chichi-0°	**Northridge-0°**	**El4 Centro-0°**	**El Centro-37°**
Post-excavation Sig-1	-603.91	-439.53	-386.68	-545.7
Pre-excavation Sig-1	-601.65	-416.53	-370.17	-558.48
Difference (%)	-3.25	5.52	4.46	-2.29

the earthquake. In the case of the Chichi-0° earthquake, Sig-1 decreased by 3.25% after excavation, which suggests that this reduction, due to an increase in compressive forces, could contribute to improved structural stability and reduce the impact of seismic forces [4]. Conversely, for the Northridge-0° earthquake, Sig-1 increased by 5.52% after excavation, indicating elevated tensile stresses that may heighten the risk of cracking and decrease structural resistance [17, 8]. Similarly, under the El Centro-0° earthquake, Sig-1 increased by 4.46%, pointing to a rise in tensile forces that could reduce the foundation's safety. For the El Centro-37° earthquake, a decrease of 2.29% in Sig-1 after excavation was observed, leading to an increase in compressive forces in the foundation and lowering the likelihood of cracks and permanent deformations. These findings align with studies that highlight the positive impact of excavation in reducing tensile forces and increasing compressive stresses [32, 3].

Overall, the results indicate that excavation can have different impacts on stress distribution and the stability of the citadel foundation depending on the earthquake's type and direction. In certain cases, excavation can improve stability by reducing tensile stress, but in earthquakes with specific angles, increased tensile forces may lead to a higher risk of seismic damage. Therefore, for sensitive structures in seismically active areas, careful consideration of possible seismic wave angles and characteristics is essential to avoid adverse stress changes and ensure foundation stability.

5 Conclusions

This study comprehensively examines the effects of seismic wave scattering on the stability and stress distribution in the foundation of a castle, particularly considering the impact of excavation near twin tunnels in earthquake-prone regions. By analyzing horizontal and overall displacements as well as stress variations across various earthquake scenarios, this research provides extensive insights into the complex interaction between seismic forces, excavation activities, and the structural behavior of historical foundations. The analysis of displacements reveals that excavation significantly influences both horizontal and overall displacements of the castle. These changes are highly dependent on the type of earthquake and the angle of wave incidence. For instance, in the ChiChi-0° earthquake scenario, there is a substantial increase of 33.72% in horizontal displacement after excavation, suggesting that certain characteristics of seismic waves can amplify the structural sensitivity. Similarly, the El Centro-37° earthquake resulted in a 23.68% increase in overall displacement due to the angle of wave incidence, highlighting the importance of wave orientation in wave-structure interaction. These findings indicate that specific angles and types of seismic waves can induce more pronounced responses in the foundation, potentially increasing displacements and risking structural integrity [32, 8, 26].

The stress analysis shows that excavation has varying effects on horizontal stress (Sig-xx) and principal stress (Sig-1) in different seismic events. For example, in the ChiChi-0° earthquake, a 3.25% decrease in horizontal stress after excavation suggests that excavation leads to a redistribution of tensile forces, potentially enhancing the stability of the foundation by reducing stress concentration. However, during the Northridge-0° and El Centro-37° earthquakes, horizontal stresses increased by 2.60% and 2.65%, respectively, indicating an increase in tensile forces that could raise the likelihood of cracking and deformation of the foundation. Moreover, the El Centro-0° earthquake showed almost no significant change in horizontal stress (0.01%), implying that certain seismic waves with lower angles of incidence may have minimal effects on stress distribution. These variations in stress responses indicate that excavation, depending on wave characteristics, angle, and seismic energy, can either decrease or increase stress concentration [26, 31].

The findings related to principal stress (Sig-1) indicate that the impact of excavation on structural stability varies with seismic conditions. In the ChiChi-0° scenario, Sig-1 decreased by 3.25% after excavation, likely due to an increase in compressive forces that enhance structural resistance against seismic forces. Conversely, in the Northridge-0° earthquake, there was a 5.52% increase in Sig-1 after excavation, reflecting higher tensile forces that may compromise stability. Similarly, a 4.46% increase in Sig-1 during the El Centro-0° earthquake indicates higher tensile stresses, potentially reducing safety margins. These changes suggest that excavation in certain seismic conditions could increase structural vulnerability, particularly when seismic waves at specific angles generate higher tensile stresses [11, 6]. The overall results show that the highest level of scattering for twin tunnels occurs under selected seismic waves at a wave incidence angle of $\alpha = 30°$ and $\theta = 90°$ for the tunnels. The findings also indicate that an increase in input wave velocity results in a lower rate of scattering compared to the wave's growth rate. On the other hand, for lower input wave speeds, no significant difference is observed between scattering in porous and elastic media. Multiple scattering significantly affects the Dynamic Stress Concentration Factor (DSCF) near the Biot critical frequency, especially for longitudinal (P) waves when the tunnels are close together [22, 25].

The maximum horizontal and overall displacements in the castle were found to be 33.7% and 23.7% higher, respectively, in the twin tunnel scenario compared to the no-tunnel condition. Comparing these two environmental states, axial stress in the local x-direction of the tunnel (Sig-xx) and the value of the principal stress (Sig-1) increased by 3.25% and 5.52%, respectively. This indicates that twin tunnels increase horizontal and overall displacements, as well as stresses on the structure due to scattering criteria.

The findings suggest that underground tunnels, cavities, and their interactions should be thoroughly considered in seismic assessments of structures, especially historical buildings. It is noteworthy that the proposed method is not limited to twin tunnels but can be applied to a wide range of conditions, particularly when variations arise from damage-sensitive features influenced by the scattering phenomenon. Statistical analysis further revealed that considering tunnel scattering behaviour has the most significant impact on adjacent structures. This study emphasizes the need for a detailed examination of the effects of excavation on structural dynamics in seismic regions, particularly near cultural heritage sites. The results underscore the importance of analyzing wave characteristics and incidence angles to better understand stress and displacement responses. The present research provides practical guidelines for planning excavation and constructing underground facilities near historical sites, where specific seismic profiles and orientations may pose unique risks [29].

This study highlights that excavation near large historical foundations in seismic zones requires a precise understanding of seismic wave behaviour, including the angle, type, and energy of potential earthquakes. Considering these factors during the design and planning stages is crucial for ensuring seismic resilience and preserving cultural and historical structures. The comprehensive approach in this study for analyzing displacements and stresses encourages further research to explore the impact of wave angles and structural responses, laying a solid foundation for seismic protection and safety of historical sites. To mitigate seismic risks from excavation near historical structures, the study offers several recommendations:

1. Targeted Strengthening Strategies: These should take into account seismic wave characteristics and incidence angles.
2. High-Strength Materials: Utilizing these in high-stress areas can help reduce the risk of damage.
3. Pre-Excavation Dynamic Analysis: Conducting these analyses can help predict stress distribution and structural response.
4. Real-Time Seismic Monitoring Systems: Installing these can provide timely data for immediate intervention.
5. Flexible Foundation Design: This would help redistribute stresses effectively.
6. Staged Excavation Methods: Implementing these techniques can control stress distribution during the excavation process.

References

[1] M. Abramowitz, I. Stegun, and D.A. McQuarrie, *Handbook of mathematical functions*, Amer. J. Phys. **34** (1966), no. 2, 177–183.

[2] M. Afifipour, M. Sharifzadeh, K. Shahriar, and H. Jamshidi, *Interaction of twin tunnels and shallow foundation at Zand underpass, Shiraz metro, Iran*, Tunnel. Underground Space Technol. **26** (2011), no. 2, 356–363.

[3] H. Alielahi, M. Kamalian, and M. Adampira, *Seismic ground amplification by unlined tunnels subjected to vertically propagating SV and P waves using BEM*, Soil Dyn. Earthquake Engin. **71** (2015), 63-79.

[4] J. Antonio and A. Tadeu, *3D scattering by multiple cylindrical cavities buried in an elastic formation*, Eur. J. Mech.-A/Solids **20** (2001), no. 3, 367–383.

[5] O. Aydan, N. Malistani, R. Ulusay, and H. Kumsar, *The damage and response of some underground structures by the 2023 February 6 Great Turkish Earthquakes and some considerations*, Engin. Geol. **336** (2024), 107549.

[6] M.H. Baziar, M.R. Moghadam, D.S. Kim, and Y.W. Choo, *Effect of underground tunnel on the ground surface acceleration*, Tunnel. Underground Space Technol. **44** (2014), 10–22.

[7] C.A. Davis, V.W. Lee, and J.P. Bardet, *Transverse response of underground cavities and pipes to incident SV waves*, Earthquake Engin. Struct. Dyn. **30** (2001), no. 3, 383–410.

[8] M. Dravinski and M. C. Yu, *Scattering of plane harmonic SH waves by multiple inclusions*, Geophys. J. Int. **186** (2011), no. 3, 1331–1346.

[9] M. Esmaeili, S. Vahdani, and A. Noorzad, *Dynamic response of lined circular tunnel to plane harmonic waves*, Tunnel. Underground Space Technol. **21** (2006), no. 5, 511–519.

[10] X.Q. Fang, H.X. Jin, and B.L. Wang, *Dynamic interaction of two circular lined tunnels with imperfect interfaces under cylindrical P-waves*, Int. J. Rock Mech. Min. Sciences . **79** (2015), 172–182.

[11] S.M. Hasheminejad and R. Avazmohammadi, *Harmonic wave diffraction by two circular cavities in a poroelastic formation*, Soil Dyn. Earthquake Engin. **27** (2007), no. 1, 29–41.

[12] L. Huang, Z. Liu, C. Wu, and J. Liang, *The scattering of plane P, SV waves by twin lining tunnels with imperfect interfaces embedded in an elastic half-space*, Tunnel. Underground Space Technol. **85** (2019), 319–330.

[13] E.A. Ivanov, *Diffraction of Electromagnetic Waves on Two Bodies*, National Aeronautics and Space Administration, 1959.

[14] R.B. Jishnu and R. Ayothiraman, *Interaction of urban underground twin metro tunnels under static and earthquake loading*, J.ournal of Earthquake Tsunami **14** (2020), no. 4, 2050019.

[15] C.Z. Karakostas and G.D. Manolis, *Dynamic response of tunnels in stochastic soils by the boundary element method*, Engin. Anal. Boundary Elements **26** (2002), no. 8, 667-680.

[16] H. Khabbaz, R. Gibson, and B. Fatahi, *Effect of constructing twin tunnels under a building supported by pile foundations in the Sydney central business district*, Underground Space **4** (2019), no. 4, 261–276.

[17] R. Khandan, A. Sivandipour, and E.A. Noroozinejad Farsangi, *Parametric study on improved reduced beam section connections with post-tensioning to enhance seismic resilience*, Int. J. Engin. **36** (2023), no. 10, 1857–1867.

[18] V.W. Lee and M.D. Trifunac, *Response of tunnels to incident SH-waves*, J. Engin. Mech. Divis. **105** (1979), no. 4, 643–659.

[19] J.C. Li, H.B. Li, G.W. Ma, and Y.X. Zhou, *Assessment of underground tunnel stability to adjacent tunnel explosion*, Tunnel. Underground Space Technol. **35** (2013), 227–234.

[20] Q. Liu and R. Wang, *Dynamic response of twin closely-spaced circular tunnels to harmonic plane waves in a full space*, Tunnel. Underground Space Technol. **32** (2012), 212–220.

[21] Q. Liu, M. Zhao, and L. Wang, *Scattering of plane P, SV or Rayleigh waves by a shallow lined tunnel in an elastic half space*, Soil Dyn. Earthquake Engin. **49** (2013), 52–63.

[22] M. Mazloom and N. Fallah, *A new approach for seismic damage detection based on results of pushover analysis and modal based damage index*, Int. J. Engin. **36** (2023), no. 10, 1892–1907.

[23] F. Mehri, S. Mollaei, E. Noroozinejad Farsangi, M. Babaei, and F. Ghahramani, *Application of a novel optimization algorithm in design of lead rubber bearing isolation systems for seismic rehabilitation of building structures*, Int. J. Engin. **36** (2023), no. 3, 594–603.

[24] I.D. Moore and F. Guan, *Three-dimensional dynamic response of lined tunnels due to incident seismic waves*, Earthquake Engin. Struct. Dyn. **25** (1996), no. 4, 357–369.

[25] A. Naseem, W.S. Ansari, M. Kashif, S. Sadiq, K. Schotte, and H. De Backer, *Evaluating the performance of the twin tunnel complex in soft soil subjected to horizontal ground shaking*, Front. Envir. Sci. **11** (2023), 1242296.

[26] A. Naseem, M. Kashif, N. Iqbal, K. Schotte, and H. De Backer, *Seismic behavior of triple tunnel complex in soft soil subjected to transverse shaking*, Appl. Sci. **10** (2020), no. 1, 334–349.

[27] Y.H. Pao and C.C. Mow, *Diffraction of elastic waves and dynamic stress concentrations*, J. Appl. Mech. **40** (1973), no. 4, 872–874.

[28] S.L. Parvanova, P.S. Dineva, G.D. Manolis, and F. Wuttke, *Seismic response of lined tunnels in the half-plane with surface topography*, Bull. Earthquake Engin. **12** (2014), 981–1005.

[29] A. Rabiefar, H. Vosoughifar, A. Nabizadeh, and H. Negahdar, *Analytical approach to scattering of P, SV waves by twin tunnels in saturated half-space*, Arch. Appl. Mech. **93** (2023), no. 2, 445–66.

[30] H. Rajabnejad, H. Hamidi, S. Naseri, and M. Abbaszadeh, *Effect of intensity measures on the response of a 3D-structure under different ground motion duration*, Int. J. Engin. **34** (2021), no. 10, 2219–2237.

[31] A. Rodríguez-Castellanos, F. Luzón, and F.J. Sánchez-Sesma, *Diffraction of seismic waves in an elastic, cracked halfplane using a boundary integral formulation*, Soil Dyn. Earthquake Engin. **25** (2005), no. 11, 827–837.

[32] D.H. Tsaur and K.H. Chang, *Multiple scattering of SH waves by an embedded truncated circular cavity*, J. Marine Sci. Technol. **20** (2012), no. 1.

[33] H. Vosoughifar, F. Madadi, and A. Rabiefar, *Modified dynamic stress concentration factor for twin tunnels using a novel approach of FEM-scattering*, Tunnel. Underground Space Technol. **70** (2017), 30–41.

[34] J.H. Wang, X.L. Zhou, and J.F. Lu, *Dynamic stress concentration around elliptic cavities in saturated poroelastic soil under harmonic plane waves*, Int. J. Solids Struct. **42** (2005), no. 14, 4295–310.

[35] C. Xin, W. Feng, D. Song, S. Huang, and X. Liu, *Seismic damage to non-fault-crossing and fault-crossing tunnels: Comparative study of the 2008 Wenchuan earthquake (Mw 7.9) and the 2022 Menyuan earthquake (Mw 6.7)*, Engin. Failure Anal. **166** (2024), 108843.

[36] N. Zhang, X. Chen, Y. Gao, and D. Dai, *Analytical solution to scattering of SH waves by a circular lined tunnel embedded in a semi-circular alluvial valley in an elastic half-space*, Tunnel. Underground Space Technol. **106** (2020), 103615.

[37] R. Zomorodian, F. Soltani, A. Sivandi-Pour, and E. Noroozinejad Farsangi, *Effect of foundation flexibility on the seismic performance of a high-rise structure under far-field and near-field earthquakes*, Int. J. Engin. **34** (2021), no. 7, 1611–1622.